

1 **Supporting Text: Power Spectra Reveal the Influence of Stochasticity on Nonlinear**  
2 **Population Dynamics**

3  
4 Daniel C. Reuman, Robert A. Desharnais, Robert F. Costantino, Omar S. Ahmad, Joel E.  
5 Cohen  
6

7 **Contents**

8 1: Methods

9 1.1: Models and parameter values..... 2  
10 1.2: Power spectrum fit tests.....2  
11 1.3: Non-equivalency of fit in the time and frequency domains.....3  
12 1.4: Lag metric and relative lag metric..... 5  
13 1.5: Extraction and significance of the length-7 pattern..... 6  
14 1.6: Plotting spectral peaks versus  $\Sigma$  factor (Fig. 4)..... 7  
15 1.7: Linearization theory..... 8  
16 1.8: Computations..... 9

17 2: Supporting Results

18 2.1: Frequency-domain fit and predictive ability of the  
19 LSD-LPA model..... 10  
20 2.2: Fits of constrained models..... 10  
21 2.3: Analogues of Fig. 4 for other life stages and  $c_{pa}$  values..... 12  
22 2.4: Limiting behavior of deterministic models for  $c_{pa} = 0$ ..... 12  
23 2.5: Explanation of spectral changes with stochasticity..... 12  
24 Supplementary References:..... 14  
25  
26

## 27 1: Methods

28

### 29 1.1: Models and parameter values

30

31 **Figure 5:** Models of *T. castaneum* population dynamics. The deterministic Larvae-  
32 Pupae-Adult model (LPA) is presented in the upper left corner, box [1]. The stochastic  
33 demographic Larvae-Pupae-Adult model (SD-LPA) is displayed in the upper right  
34 corner, box [2]. The lattice stochastic demographic Larvae-Pupae-Adult model (LSD-  
35 LPA) is shown in the lower right corner, box [3]. We consider the LSD-LPA model to be  
36 assembled starting with the LPA model, adding stochasticity first, then constraining to  
37 integer populations, rather than *vice versa*.  $[x] = \max(x, 0)$ . The trivariate random  
38 variables  $E_t = (E_{1t}, E_{2t}, E_{3t})$  were standard normal with covariance matrix  $\Sigma$ , and were  
39 independent for different values of  $t$ . *See separate file for the figure.*

40

41 **Table 1:** The parameters used for the models of Fig. 5. These were obtained using time  
42 domain fitting methods (Dennis *et al.* 2001, Cushing *et al.* 2003). *See separate file for the*  
43 *table.*

44

### 45 1.2: Power spectrum fit tests

46 The “spectrum distance fit test” quantifies the frequency-domain fit between a model  
47 with specified parameters and an experimental time series,  $\{x_0, \dots, x_{T-1}\}$ . Steps for  
48 computing the  $p$ -value result of the test for a population model and data with life stages  
49 L, P and A are:

50

- 51 • Use the model with initial conditions  $x_0$  to produce  $N$  simulated time series of length  
52  $T$ .
- 53 • Compute the log spectral estimate  $\log(f_X^{(T)}(\lambda))$  of each life stage of each simulated  
54 time series ( $3*N$  log spectra) using a “consistent spectral estimate” of Brillinger  
55 (Brillinger 2001, p. 146). The variable  $\lambda$  denotes normalized frequency (n.f.).
- 56 • For each  $\lambda = 2s/T$  (for  $s$  an integer from 0 to  $\lfloor T/2 \rfloor$ ), and for each life-stage, compute  
57 the mean of the  $N$  values of  $\log(f_X^{(T)}(\lambda))$  that were computed for that life stage. Call  
58 the resulting three spectra (one for each life-stage) the “mean model log spectra,”  
59  $\bar{u}_L^{(T)}(\lambda)$ ,  $\bar{u}_P^{(T)}(\lambda)$  and  $\bar{u}_A^{(T)}(\lambda)$ .
- 60 • For each log spectrum of a model-generated time series (the three life-stage  
61 components of which we denote  $u_L^{(T)}(\lambda)$ ,  $u_P^{(T)}(\lambda)$  and  $u_A^{(T)}(\lambda)$ ) compute the three  
62 distances:

63

**Eqn. 1** 
$$d_w(u_w, \bar{u}_w) = \sqrt{\sum_{s=0}^{\lfloor T/2 \rfloor} (u_w^{(T)}(2s/T) - \bar{u}_w^{(T)}(2s/T))^2}$$

64

for  $w = L, P, A$ . Let

65

$$d(u, \bar{u}) = \sqrt{\sum_{w=L,P,A} d_w(u_w, \bar{u}_w)^2} .$$

66

This  $d(u, \bar{u})$  gives  $N$  points from a distribution of  $d$ .

67

- 67 • Denote log-spectra of the life-stage components of the experimental data time series  
68 by  $e_L^{(T)}(\lambda)$ ,  $e_P^{(T)}(\lambda)$ ,  $e_A^{(T)}(\lambda)$ , and compute  $d(e, \bar{u})$ .

- 69 • Generate an approximate  $p$ -value from the  $d$  distribution for this experimental  
 70 replicate by computing the percentage of the  $d(u, \bar{u})$  that are greater than  $d(e, \bar{u})$ .  
 71

72 The distance in Eqn. 1 is the square root of the sum of the squared differences between  
 73 the mean model spectrum values  $\bar{u}_w(2s/T)$  and the individual spectrum values  $u_w(2s/T)$ .  
 74 This quantity is small when the spectra  $u_w$  and  $\bar{u}_w$  are close for all values of  $s$   
 75 simultaneously.

76 Steps for computing the  $p$ -value result of the “spectrum shape fit test” for a  
 77 population model and data with life stages L, P and A are:  
 78

- 79 • Use the model with initial conditions  $x_0$  to produce  $N$  simulated time series of length  
 80  $T$ .  
 81 • Compute the log spectral estimate  $\log(f_X^{(T)}(\lambda))$  of each life stage of each simulated  
 82 time series ( $3*N$  log spectra) using a “consistent spectral estimate” of Brillinger  
 83 (Brillinger 2001, p. 146). The variable  $\lambda$  denotes normalized frequency (n.f.).  
 84 • For each  $\lambda = 2s/T$  (for  $s$  an integer from 0 to  $\lfloor T/2 \rfloor$ ), and for each life-stage, compute  
 85 the mean of the  $N$  values of  $\log(f_X^{(T)}(\lambda))$  that were computed for that life stage. Call  
 86 the resulting three spectra (one for each life-stage) the "mean model log spectra,"  
 87  $\bar{u}_L^{(T)}(\lambda)$ ,  $\bar{u}_P^{(T)}(\lambda)$  and  $\bar{u}_A^{(T)}(\lambda)$ .  
 88 • For each log spectrum of a model-generated time series (the three life-stage  
 89 components of which we denote  $u_L^{(T)}(\lambda)$ ,  $u_P^{(T)}(\lambda)$  and  $u_A^{(T)}(\lambda)$ ) compute the three  
 90 correlation coefficients  $c(u_w^{(T)}(\lambda), \bar{u}_w^{(T)}(\lambda))$  for  $w = L, P, A$ , and compute their sum,  
 91  $c(u, \bar{u})$ . This gives  $N$  points from a distribution of  $c$  values.  
 92 • Denote log-spectra of the life-stage components of the experimental data time series  
 93 by  $e_L^{(T)}(\lambda)$ ,  $e_P^{(T)}(\lambda)$ ,  $e_A^{(T)}(\lambda)$ , and compute  $c(e, \bar{u})$ .  
 94 • Generate an approximate  $p$ -value from the  $c$  distribution for this experimental  
 95 replicate by computing the percentage of the  $c(u, \bar{u})$  that are less than  $c(e, \bar{u})$ .  
 96

97 These tests give approximate  $p$ -values because they are based on stochastic  
 98 simulation: executing the same steps twice gives slightly different results. For this study,  
 99 every  $p$ -value was computed 100 times, and means and standard deviations of the  
 100 resulting distribution of approximate  $p$ -values were computed, as well as minima, 25<sup>th</sup>,  
 101 50<sup>th</sup>, and 75<sup>th</sup> percentiles, and maxima. The variance of the  $p$ -value distributions obtained  
 102 from the tests can be decreased by increasing  $N$ . Typical values of  $N$  used in this study  
 103 were 5000 and 10,000.

104 A model for which the 25<sup>th</sup> percentile of a  $p$ -value distribution from one of the  
 105 two tests above was bigger than 1% was considered to be well-fitting with respect to that  
 106 test. Models that fit for both tests using this criterion produced time series with power  
 107 spectra that looked visually very similar to those of the data time series (e.g., Fig. 2 A, B,  
 108 C, E but not D, F).  
 109

### 110 **1.3: Non-equivalency of fit in the time and frequency domains**

111 A model that had good one-time-step forecasting ability did not always have to fit well in  
 112 the frequency domain according to the spectrum distance fit test, nor conversely. A  
 113 stochastic version of the Ricker model,

114 
$$p_{n+1} = 17 * p_n \exp\left(-\frac{1}{300} p_n + 0.03 * X_n\right),$$

115 was used to generate three data time series  $d_1, d_2, d_3$  of length 128 starting from initial  
 116 condition  $p_0 = 14$ . The  $X_n$  were independent standard normal. One-step-forecasting  
 117 maximum-likelihood techniques similar to those used in Cushing *et al.* (2003) were used  
 118 to fit the model

119 
$$p_{n+1} = 17 * p_n \exp\left(-\frac{c}{300} p_n + 0.13 * X_n\right)$$

120 with  $d_1, d_2, d_3$  (the coefficient 0.13 was intentionally different from the coefficient 0.03 in  
 121 the above model); the best-fitting model had  $c \approx 1$ . The spectrum distance fit test found  
 122 best-fitting  $c \approx 1.24$ . In the frequency domain, the model with  $c = 1$  had  $p = 0.02\%$   
 123 (spectrum distance fit test); the model with  $c = 1.24$  had  $p = 7.76\%$  (spectrum distance fit  
 124 test). P-values of three replicates were combined into a single p-value by the Fisher  
 125 method. The time-domain likelihood function evaluated at  $c = 1$  was about  $1.7 \times 10^{181}$ ;  
 126 evaluated at  $c = 1.24$  it was less than  $10^{-10}$ . Thus the time-domain fitting indicates that  $c =$   
 127  $1.24$  is much less likely than  $c = 1$ , while the spectrum distance fit test indicates the  
 128 reverse.

129 A second-order-Markov relative of the stochastic Ricker model was used to  
 130 generate three data time series  $e_1, e_2, e_3$  of length 128 starting from initial conditions  $p_0 =$   
 131  $14, p_1 = 227.1485$ :

132 
$$p_{n+1} = (17 * p_n + 0.1 * p_{n-1}) \exp\left(-\frac{1}{300} p_n + 0.03 * X_n\right).$$

133 The dependence of  $p_{n+1}$  on  $p_{n-1}$  can be interpreted as some eggs laid during time step  $n-1$   
 134 not hatching until time step  $n+1$ , although most hatch during time step  $n$ . The parameters  
 135 17 and 0.1 in this model correspond to the biological hypothesis that  $17/(17+0.1) =$   
 136  $99.42\%$  of eggs hatch after one time step, while the rest hatch after two time steps. One-  
 137 step-forecasting maximum-likelihood techniques similar to those used in Cushing *et al.*  
 138 (2003) were used to fit the model

139 
$$p_{n+1} = b * p_n \exp\left(-\frac{1}{300} p_n + \sigma * X_n\right)$$

140 with  $e_1, e_2, e_3$ . This model corresponds to the reasonable but inaccurate biological  
 141 hypothesis that all eggs hatch after one time step. The best-fitting model had  $b \approx 17.62$   
 142 and  $\sigma \approx 0.0688$ . The spectrum distance fit test found best-fitting  $b \approx 16.60$  and  $\sigma \approx$   
 143  $0.0113$ ; these parameters gave  $p = 15.24\%$  in the frequency domain (spectrum distance fit  
 144 test). The parameters  $b \approx 17.62$  and  $\sigma \approx 0.0688$  gave  $p = 0.56\%$  in the frequency domain  
 145 (spectrum distance fit test). P-values of three replicates were combined into a single p-  
 146 value by the Fisher method. The time-domain likelihood function evaluated at  $(b, \sigma) =$   
 147  $(17.62, 0.0688)$  was about  $2.3 \times 10^{208}$ ; evaluated at  $(b, \sigma) = (16.60, 0.0113)$  it was less than  
 148  $10^{-10}$ .

149 To show that the methods of this study are capable of rejecting reasonable model  
 150 functional forms based on data of 41-time-step length, we used the model

151 
$$p_{n+1} = (17 * p_n + 0.25 * p_{n-1}) \exp\left(-\frac{1}{300} p_n + 0.03 * X_n\right)$$

152 to generate time series  $f_1, f_2, f_3$  of length 41 starting from the initial conditions  $p_0 = 14, p_1$   
 153  $= 227.1485$ . The parameters 17 and 0.25 in this model correspond to the biological

154 hypothesis that  $17/(17+0.25) = 98.55\%$  of eggs hatch after one time step, while the rest  
 155 hatch after two time steps. One-step-forecasting maximum-likelihood techniques were  
 156 used to fit the model

$$157 \quad p_{n+1} = b * p_n \exp\left(-\frac{1}{300} p_n + \sigma * X_n\right)$$

158 with  $f_1, f_2, f_3$ . The best-fitting model had  $b \approx 18.84$  and  $\sigma \approx 0.1630$ ; the frequency domain  
 159 fit of the model with these parameters gave  $p < 0.0001$  (spectrum distance fit test; the 3 p-  
 160 values were combined via the Fisher method). The spectrum distance fit test found best-  
 161 fitting  $b \approx 16.00$ ,  $\sigma \approx 0.0767$ , with  $p = 2.44\%$ . The time-domain likelihood function  
 162 evaluated at  $(b, \sigma) = (18.84, 0.1630)$  was about  $5.0 \times 10^{-20}$ ; evaluated at  $(b, \sigma) = (16.00,$   
 163  $0.0767)$  it was less than  $10^{-10}$ . No single set of parameters  $(b, \sigma)$  produced a fit according  
 164 to both time and frequency domain measures of fit, so we reject the model.

165 We used the model

$$166 \quad p_{n+1} = (17 * p_n + 0.5 * p_{n-1}) \exp\left(-\frac{1}{300} p_n + 0.03 * X_n\right)$$

167 to generate time series  $f_1, f_2, f_3$  of length 41 starting from the initial conditions  $p_0 = 14$ ,  $p_1$   
 168  $= 227.1485$ . The parameters 17 and 0.5 in this model correspond to the biological  
 169 hypothesis that  $17/(17+0.5) = 97.14\%$  of eggs hatch after one time step, while the rest  
 170 hatch after two time steps. One-step-forecasting maximum-likelihood techniques were  
 171 used to fit the model

$$172 \quad p_{n+1} = b * p_n \exp\left(-\frac{1}{300} p_n + \sigma * X_n\right)$$

173 with  $f_1, f_2, f_3$ . The best-fitting model had  $b \approx 22.40$  and  $\sigma \approx 0.3850$ ; the frequency domain  
 174 fit of the model with these parameters gave  $p < 0.0001$  (spectrum distance fit test; 3 p-  
 175 values combined by the Fisher method). The spectrum distance fit test found best-fitting  
 176  $b \approx 16.33$ ,  $\sigma \approx 0.08$ , with  $p = 0.0009$ . Frequency domain fit was not possible with this  
 177 model functional form for any parameters in the range searched.

178

#### 179 **1.4: Lag metric and relative lag metric**

180 Two “lag metrics” were used: one developed previously (King *et al.* 2004), and an  
 181 adaptation of that method. The adapted method, called the “relative lag metric,” detected  
 182 the presence of length- $n$  approximately-periodic patterns in a time series. For the time  
 183 series  $x_0, \dots, x_{T-1}$ , the “relative lag metric” method computed

$$184 \quad D_t = \left( \sum_{i=t-n+1}^t \delta_1(x_i, x_{i-n}) \right) / n$$

185 for  $t = 2n-1$  to  $T-1$ . The notation  $\delta_1$  represented distance under the 1-norm:

$$186 \quad \delta_1((L_i, P_i, A_i), (L_j, P_j, A_j)) = |L_i - L_j| + |P_i - P_j| + |A_i - A_j|.$$

187 The quantity  $D_t$  was the average distance between  $x_i$  and  $x_{i-n}$  for  $i$  ranging over the past  $n$   
 188 time steps; low values of  $D_t$  indicated that the data had been passing through an  
 189 approximately repeating length- $n$  periodic pattern for at least the last  $2n$  time steps (one  
 190 sequence of  $n$  points followed by one approximate repetition of that sequence). The  
 191 distance  $D_t$  was plotted versus  $t$ , keeping track of the times for which it was less than 55  
 192 (the value 55 was taken from a previous application of the lag metric to the *T. castaneum*  
 193 system, King *et al.* 2004). The number of total  $t$  values for which  $D_t$  was less than 55 and

194 the maximum number of contiguous  $D_t$  values below 55 provided an indication of the  
195 degree to which approximately-repeating length- $n$  patterns occurred.

196 The original “lag metric” method (King *et al.* 2004) differed from the relative lag  
197 metric because it took a fixed length- $n$  pattern  $c^{(n)}$  as additional input. It measured the  
198 average distance between each  $n$ -long sub-time series  $x_{t-n+1}, \dots, x_t$  and  $c^{(n)}$ , and plotted  
199 this distance against  $t$ . The pattern  $c^{(n)}$  had  $n$  possible rotations; the lag metric plotted the  
200 average distance to each possible rotation, giving  $n$  different lines on a single plot. When  
201 any one of these lines was below 55 the data were considered to be approximately  
202 repeating the pattern  $c^{(n)}$ .

203

### 204 **1.5: Extraction and significance of length-7 pattern**

205 This section gives the details of how an approximately-repeating pattern of length 7 was  
206 extracted from LSD-LPA model output and from experimental data with  $c_{pa} = 0$ , and how  
207 the statistical significance of the presence of that pattern was determined. An  
208 approximately repeating pattern of length 6 was extracted from model output and  
209 experimental data with  $c_{pa} = 0.5$  using the same methods.

210

211 Extraction:

212 Starting with length-1024 output of the LSD-LPA model with  $c_{pa} = 0$  and  $\mu_a =$   
213 0.96, and other parameters equal to those of Table 1, all time steps for which the relative  
214 lag metric, with lag 7 (Section 1.4), was less than 75 were found. Of these, the time steps  
215 were kept that were part of a run of length at least 8 time steps with relative lag metric  
216 below 75. Such a run indicated that the time series was executing an approximately-  
217 periodic pattern of length 7, for at least 21 time steps (3 repetitions of the pattern). For the  
218 model output used, there were no runs of length greater than 10 time steps for which the  
219 relative lag metric was below 75.

220 If  $t$  was the first time step of each run of length 8 or greater, the population triples  
221 from  $t-13$  to  $t+7$  were extracted, giving 3 potential repetitions of a length-7 pattern. In this  
222 way, 27 potential patterns of length 7 were extracted from the length-1024 series. The  
223 first of these (an arbitrary choice) was labeled  $x$ . For  $y$  equal to each of the 26 other  
224 patterns, the average 1-norm distance between  $y$  and  $x$  was measured for each of the 7  
225 possible rotations of  $y$ . The patterns  $y$  for which no rotation had distance to  $x$  less than 90  
226 were discarded. No pattern  $y$  had more than one rotation with distance to  $x$  less than 90.  
227 This one rotation “lined up” with  $x$ . After discarding the patterns for which no rotation  
228 lined up, the adult life stage of 10 of the 19 remaining patterns was plotted, randomly  
229 chosen (Fig. 3D), and the median of the 19 population values for each time step and for  
230 each life stage was computed to get one median length-7 pattern.

231 The (original) lag metric (Section 1.4) was used to compare the experimental time  
232 series from the treatment with  $c_{pa} = 0$  (replicates 5, 12 and 15) to the median length-7  
233 pattern extracted from model output. For replicates 5 and 15, the metric never went below  
234 the threshold of 55, but for replicate 12 it did so for 4 consecutive time steps, indicating  
235 that this length-7 pattern occurred in experimental data. The minimum lag metric value  
236 for replicate 12 was 40.14 individuals, and for replicate 5 it was 62.57 individuals. The 7  
237 time steps ending at the time step with minimal lag metric were extracted from replicates  
238 5 and 12, and rotated to line up with the length-7 patterns extracted from typical model  
239 output. The adult life stages of these extracted patterns were plotted (Fig. 3D).

240

241 Statistical Significance:

242 To test whether the median pattern extracted and displayed in Fig. 3D (open  
243 circles) occurred only by chance, we randomly permuted, in 1000 different ways, the  
244 same LSD-LPA model output from which the pattern was extracted. For each permuted  
245 time series, the same steps were undertaken as were used to extract the pattern from the  
246 un-permuted model output: the relative lag metric (Section 1.4) was applied to each  
247 permuted time series, and the length of the longest run of time steps for which the relative  
248 lag metric was below the threshold 75 was recorded. None of the 1000 permutations had  
249 a run longer than 6. Nine runs of length 8 or more occurred in the un-permuted model  
250 output.

251 To test whether the median pattern displayed in Fig. 3D (open circles) was  
252 detected in experimental replicates 5 and 12 by chance alone, we randomly permuted, in  
253 1000 different ways, the experimental time series of replicates 5 and 12, and attempted to  
254 find the same median pattern in each permuted time series using the same methods with  
255 which it was detected in un-permuted experimental data: the lag metric was used to test  
256 for the presence of the median pattern in each permuted time series. The lag metric never  
257 went below the threshold of 55 for any of the 1000 permutations for either replicate. The  
258 same test was run on data from experimental replicate 15 (same treatment group), with  
259 the same results.

260

#### 261 **1.6: Plotting spectral peaks versus $\Sigma$ factor (Fig. 4)**

262 For each of 101 log  $\Sigma$  factors evenly spaced from  $\log(2 \times 10^{-5})$  to 1, 1000 time series of  
263 length  $T = 1024$  were generated using the SD-LPA model. The log periodogram spectral  
264 estimate (Brillinger 2001) of each life stage of each time series was computed. For each  
265 n.f. value of the form  $2s/T$  for  $s$  an integer from 1 to  $\lfloor T/2 \rfloor$ , the median of the log  
266 periodogram values at that n.f. was computed for each life stage. The periodogram value  
267 at n.f. = 0 was removed before computing medians because it did not contain spectral  
268 information.

269 The resulting median log periodograms (with the n.f. = 0 value omitted) were  
270 smoothed using local averaging to eliminate small spurious peaks and valleys. The  
271 smoothing was simple averaging of the median log-periodogram value at each frequency  
272 with the values at the 10 frequencies of the form  $2s/T$  (for  $s$  an integer from 1 to  $\lfloor T/2 \rfloor$ )  
273 on each side of it. For most n.f. values, 21 quantities were averaged. The average of all  
274 available frequencies was used for normalized frequencies close to 0 or 1 not having ten  
275 frequencies on one side.

276 Locations of local maxima and minima were computed using the smoothed  
277 median log periodogram for each log  $\Sigma$  factor. A frequency was considered to be the  
278 location of a local maximum if its smoothed median log-periodogram value was at least  
279 as great as the values of the 10 frequencies on each side of it (or fewer for frequencies  
280 close to 0 and 1). Heights of the local maxima and minima were computed using the  
281 smoothed median log periodogram. Locations and heights of spectral peaks and valleys  
282 were plotted against log  $\Sigma$  factor (Fig. 4).

283 Although not all trends of peaks appearing on plots produced in this way will be  
284 biologically meaningful (some are artifacts of the spectrum method), they will all be  
285 highly statistically significant for two reasons. First, computing the median of 1000 log-

286 periodograms and subsequently smoothing the median eliminates peaks that are due to  
287 dramatic, chance departures of dynamics from central patterns. Second, the random  
288 components affecting simulations with adjacent  $\log \Sigma$  factors are independent. Although  
289 a statistically rare and not dynamically meaningful peak may occasionally occur for a  
290 single value of the  $\log \Sigma$  factor, the probability that an entire trend of peaks will  
291 materialize by chance is vanishingly small.

292

### 293 **1.7: Linearization theory**

294 Theory based on linearization uses the power spectrum to explain interactions between  
295 stochasticity and nonlinear dynamics in physical systems (Wiesenfeld 1985) and  
296 population models (Greenman & Benton 2005). We briefly review the main qualitative  
297 conclusions of the theory. Given a deterministic model  $\mathbf{x}_{t+1} = f(\mathbf{x}_t)$  with a finite stable  
298 attractor  $A = (\mathbf{x}_1, \mathbf{x}_2, \dots, \mathbf{x}_n)$  consisting of  $n$  points periodically repeated, the spectral  
299 effects of adding normally-distributed stochasticity  $\boldsymbol{\varepsilon}$  to the model,  $\mathbf{x}_{t+1} = f(\mathbf{x}_t) + \boldsymbol{\varepsilon}$ , can be  
300 predicted from the eigenvalues and eigenvectors of the “susceptibility matrix”

301  $S = J_{\mathbf{x}_n} J_{\mathbf{x}_{n-1}} \dots J_{\mathbf{x}_1}$ , where  $J_{\mathbf{x}}$  is the Jacobian of  $f$  at  $\mathbf{x}$ . A negative real eigenvalue  $d_1$  with  
302 corresponding eigenvector  $\mathbf{v}$  indicates that small perturbations  $\mathbf{h}$  from  $\mathbf{x}_1$  in the direction  
303 of  $\mathbf{v}$  will become, in  $n$  time steps, approximately  $S\mathbf{h} = d_1\mathbf{h}$ , which has direction opposite  
304 that of  $\mathbf{h}$ . This direction switching of perturbations has period  $2n$ , twice that of the  
305 deterministic system. It is over-compensatory decay of the perturbation  $\mathbf{h}$ . If  $\boldsymbol{\varepsilon}$  has a  
306 component in the direction of  $\mathbf{v}$ , and  $\mathbf{v}$  has non-zero  $i^{\text{th}}$  component, then direction  
307 switching of perturbations (over-compensatory decay) causes a stochastically-induced  
308 peak in the spectrum of the  $i^{\text{th}}$ -component time series at n.f.  $1/n$  (half the frequency of the  
309 deterministic system if  $n > 1$ , because the deterministic system has n.f.  $2/n$ ).

310 If  $S$  has a complex-conjugate pair of eigenvalues  $d_1$  and  $d_2$  with phase angles  $\alpha$   
311 and  $-\alpha$ , then there is a 2-dimensional space  $\mathbf{V}$  such that  $S$  approximately rotates vectors in  
312  $\mathbf{V}$  by average angle  $\alpha$  and then re-scales them by  $|d_1|$ . Perturbations  $\mathbf{h}$  from  $\mathbf{x}_1$  that lie in  $\mathbf{V}$   
313 will be approximately  $S\mathbf{h}$  in  $n$  time steps: they will be approximately rotated by  $\alpha$  and  
314 multiplied by  $|d_1|$ . This amounts to oscillatory decay of the perturbation  $\mathbf{h}$ , with  
315 oscillations of n.f.  $\alpha/\pi n$ . If stochasticity produces perturbations with components in  $\mathbf{V}$ ,  
316 and if  $\mathbf{V}$  contains vectors with non-zero  $i^{\text{th}}$  component, then rotation causes a  
317 stochastically-induced peak at n.f.  $\alpha/\pi n$  in the spectrum of the  $i^{\text{th}}$ -component time series.  
318 Because rotation by  $\alpha$  is the same as rotation by  $2\pi - \alpha$  in the other direction, a second  
319 peak at  $(2\pi - \alpha)/\pi n$  also occurs if  $n > 1$ .

320 If  $S$  has a positive real eigenvalue  $d_1$  with corresponding eigenvector  $\mathbf{v}$ , then small  
321 perturbations  $\mathbf{h}$  from  $\mathbf{x}_1$  in the direction of  $\mathbf{v}$  will become approximately  $d_1\mathbf{h}$  in  $n$  time  
322 steps. By the assumed stability,  $d_1 < 1$ , so perturbations  $\mathbf{h}$  decay exponentially over time,  
323 with larger  $d_1$  causing slower decay. The decay is under-compensatory. If  $\boldsymbol{\varepsilon}$  has a  
324 component in the direction of  $\mathbf{v}$  and  $\mathbf{v}$  has non-zero  $i^{\text{th}}$  component, then under-  
325 compensatory decay of perturbations produces reddening in the  $i^{\text{th}}$ -component time  
326 series: spectral power increases at low frequencies.

327 Because  $A$  is stable, all eigenvalues have magnitude less than 1. Larger eigenvalue  
328 magnitudes cause larger stochastically-induced peaks for any combination of  
329 eigenvalues. Larger stochasticity also causes larger peaks, up to the limit where  
330 linearization theory begins breaking down. Linearization theory also makes quantitative

331 spectral predictions (Wiesenfeld 1985; Greenman & Benton 2005); this study makes use  
332 of qualitative predictions only.

333

### 334 **1.8: Computations**

335 All logarithms were base 10. The Matlab function ‘fft’ was used for discrete Fourier  
336 transforms. All computations were done on a 3.2 GHz desktop PC using Matlab versions  
337 6.5.0 and 6.5.1, with one exception. An adaptation of the Nelder-Mead simplex algorithm  
338 was used to optimize the LSD-LPA model fit starting from parameters of Table 1. This  
339 algorithm was run on a cluster of 16 PC machines of 1.5 GHz each. The Matlab C  
340 compiler was used to translate code to the C programming language for this purpose. The  
341 algorithm was stochastic, so it was repeated many times. The computational power of the  
342 cluster of 16 machines was needed for this repetition.

## 343 2: Supporting Results

344

### 345 2.1: Frequency-domain fit and predictive ability of the LSD-LPA model

346 Using model parameters obtained by maximum-likelihood time-domain fitting (Section  
347 1.1), the frequency-domain fit of the LSD-LPA model with all 24 data replicates was  
348 tested (Fig. 1, box 2). The six replicates of length 213 were truncated to length 41 for this  
349 purpose. The fit-testing algorithms were based on stochastic simulations, so multiple tests  
350 of fit with the same data and parameters produced slightly different  $p$ -values; but the  
351 standard deviation of  $p$ -values for 100 tests was never more than 1.25% for any replicate,  
352 for both the spectrum distance fit test and the spectrum shape fit test. All replicates but  
353 one for the spectrum distance fit test and two for the spectrum shape fit test had at least  
354 75 of 100 approximate  $p$ -values above 1%. For all replicates and life stages, visual  
355 confirmation of fit was obtained (Fig. 2A). An adaptation of the Nelder-Mead simplex  
356 algorithm was used to make small modifications of parameters to decrease the  $L_2$   
357 distances between data log spectra and the mean of log spectra of model-generated time  
358 series. No significant improvement in frequency-domain fit occurred (according to the  
359 spectrum distance fit test). The model fitted better with the given parameters than with  
360 any nearby parameters; it fitted data well in both the time and frequency domains with  
361 the same parameters.

362 Spectral estimates from length-41 time series lack resolution. To make spectral  
363 predictions of higher resolution, we generated many time series of length 213 using the  
364 LSD-LPA model (parameter values were the same as those of Section 1.1); spectral  
365 estimates based on these time series were model-based hypotheses of population spectra  
366 (Fig. 1, box 3). We tested the predictive ability of the model and the strategy of this study  
367 (Fig. 1, fourth box) by comparing these hypotheses with spectral estimates from the 6  
368 experimental replicates of length 213 (control and  $c_{pa}=0.35$  replicates). Hypotheses and  
369 data-based estimates agreed qualitatively and quantitatively: a second spectral peak at  
370 normalized frequency (n.f.) 0.33 was predicted by the model and confirmed by the  
371 length-213 experimental time series for  $c_{pa}=0.35$  (Fig. 2B); every replicate had at least 75  
372 of 100 approximate- $p$ -values above 1% for both spectrum fit tests. Standard deviations of  
373  $p$ -value distributions were always less than 0.7%.

374

### 375 2.2: Fits of constrained models

376 We examined the fit in the time and frequency domains between several variants of the  
377 LSD-LPA model and the three experimental replicates with imposed  $c_{pa} = 0.35$ . Models  
378 used were: the constrained LSD-LPA model; and the constrained LSD-LPA model with  
379 additional constraints  $c_{el} = 0$  and  $c_{ea} = 0$ , imposed separately. Parameters were computed  
380 that produced the best time-domain fit between each model and the three experimental  
381 replicates truncated to length 41 (Table 2). For all models, the time-domain-optimal  
382 parameters also gave a good fit with short time series in the frequency domain, according  
383 to both the spectrum distance fit test and the spectrum shape fit test (Table 3).

384 An adapted Nelder-Mead simplex algorithm was used to adjust model parameters  
385 to decrease the  $L_2$  distance between log spectra of short experimental time series (length  
386 41) and the mean of log spectra of many model-generated time series of the same length;  
387 the goal was to optimize frequency-domain fit. Because the algorithm optimized a  
388 stochastic objective function, it was run 5 times for each model, starting from initial

389 parameters equal to the time-domain optimum. Results represent local minima of the  
390 mean of the stochastic objective function. Frequency-domain-optimized parameters often  
391 produced a slightly but not substantially better frequency-domain fit than did the time-  
392 domain-optimal parameters (Table 3); they sometimes fell outside the 99% confidence  
393 intervals of the time-domain-optimal parameters (Table 2).

394 Models with optimized parameters were used to generate many time series of  
395 length 213; the log spectra of these long time series were compared with log spectra of  
396 the three length-213 experimental time series with imposed  $c_{pa} = 0.35$ . P-values were  
397 produced describing the degree of similarity between model and experimental spectra  
398 (Table 3); these p-values reflect the ability of each model to make accurate predictions of  
399 spectra of long time series when optimized using short time series. Both time-domain-  
400 optimized and frequency-domain-optimized parameters were used, separately. The  
401 constrained LSD-LPA model was the only model capable of making accurate predictions,  
402 although all models fitted adequately with short time series in the time and frequency  
403 domains. This difference in predictive ability of the models arises because the  
404 constrained LSD-LPA model is the only model, among those considered here, that did  
405 not incorrectly omit a known biological mechanism.

406 The analytic strategy of this study (Fig. 1) combines the qualitative, biological  
407 information contained in a model functional form with quantitative information contained  
408 in short time series to produce the best available estimate of population spectra. A  
409 mechanistic model with the wrong mechanism will produce incorrect spectral predictions  
410 for long time series even though it may fit well with short time series.

411  
412 **Table 2:** Optimized parameter values in the time domain (column 2), and in the  
413 frequency domain according to the spectrum distance fit test (columns 4-8), with respect  
414 to the length-41 experimental replicates with  $c_{pa} = 0.35$  only. Values in brackets do not  
415 fall within the confidence intervals in column 3. Time-domain fitting used the maximum  
416 likelihood one-step forecasting methods of Dennis *et al.* (2001). Frequency-domain  
417 optimization used an adaptation of the Nelder-Mead simplex algorithm to minimize the  
418 distance between the mean log spectrum of model-generated time series and data log  
419 spectra. The time-domain-optimal parameters (column 2) were used as initial conditions.  
420 Confidence intervals for the time-domain-optimal parameters other than  $\Sigma$  were  
421 computed as in Dennis *et al.* (2001). Confidence intervals for entries of  $\Sigma$  were computed  
422 by re-sampling (with replacement) from the set of residuals of data from one-step  
423 forecasts of the model with time-domain-optimal parameters. *See separate file for the*  
424 *table.*

425  
426 **Table 3:** Frequency domain fit of models with  $c_{pa} = 0.35$  data, parameters as specified in  
427 Table 2. Table entries are p-values as given by the spectrum distance fit test (columns 2-  
428 3) and the spectrum shape fit test (columns 4-5). They describe the fit between models  
429 and length-41 (columns 2, 4) or length-213 (columns 3, 5) versions of the three  $c_{pa} = 0.35$   
430 experimental time series. *See separate file for the table.*

431  
432 **Figure 6:** Frequency domain fit between the constrained LSD-LPA model (with no  
433 further constraint) and observed adult population time series of (A) length 41 and (B)  
434 length 213 from the three experimental replicates with  $c_{pa} = 0.35$ . The heavy dashed lines

435 are data log spectra. Light solid lines give the minimum, the 5<sup>th</sup>, 25<sup>th</sup>, 50<sup>th</sup>, 75<sup>th</sup>, and 95<sup>th</sup>  
436 percentiles, and the maximum values at each frequency value of 1000 log spectra of  
437 model-generated time series of (A) length 41 and (B) length 213. Triangles highlight the  
438 5th and 95th percentiles. Parameters were optimized for length-41 data in the time  
439 domain (Table 2). Fit was similar when frequency-domain-optimized parameters were  
440 used (Table 3). Fit with other life stages was similar. Aliasing of fundamental (i.e., non-  
441 harmonic) frequencies of population fluctuation is unlikely to have occurred because the  
442 biology of *Tribolium* suggests that little fluctuation occurs for n.f. greater than 1. *See*  
443 *separate file for the figure.*

444

### 445 **2.3: Analogues of Fig. 4 for other life stages and $c_{pa}$ values**

446

447 **Figure 7:** (A) Fig. 4A, reproduced here for easy comparison with the other panels. The  
448 analog of Fig. 4A for the pupal (B) and larval (C) life stages. (D) Fig. 4B, reproduced for  
449 comparison. The analogue of Fig. 4B for the pupal (E) and larval (F) life stages. *See*  
450 *separate file for the figure.*

451

452 **Figure 8:** Log power versus n.f. and log  $\Sigma$  factor,  $c_{pa} = 0$ ,  $\mu_a = 0.96$ , for the adult (A),  
453 pupal (B), and larval (C) life stages. The smoothed median log periodogram estimate was  
454 used. As in Fig. 4B and Fig. 7, n.f. = 0 values have not been plotted. This is the 3-  
455 dimensional version of Fig. 4B. There appear to be differences among Figs. 7D-F. This  
456 figure shows that the differences are minor; they may not have biological significance.  
457 *See separate file for the figure.*

458

459 **Figure 9:** Analogues of Fig. 4 for other  $c_{pa}$  values. Adult life stage only. *See separate file*  
460 *for the figure.*

461

### 462 **2.4: Limiting behavior of deterministic models for $c_{pa} = 0$**

463 The limiting behavior of the LPA model is described by its attractor (Fig. 10). This  
464 attractor, an invariant loop, consists of two small circles:  $c_1$  and  $c_2$ . All points on one of  
465 the circles have few larvae (33 to 39), many pupae (92 to 99), and few adults (30 to 35): a  
466 pupae-dominated age distribution. All points on the other circle have many larvae (115 to  
467 124), few pupae (26 to 32) and many adults (93 to 100): a bimodal age distribution.  
468 Oscillations between heavily-pupae-dominated and heavily-bimodal distributions  
469 correspond to switching between opposite sides of  $c_1$  and  $c_2$ ; oscillations between  
470 moderately-pupae-dominated and moderately-bimodal distributions correspond to  
471 switching between the sides of  $c_1$  and  $c_2$  that are closest to each other.

472

473 **Figure 10:** The attractor (circles) and unstable equilibrium (x) of the LPA model for  $c_{pa} =$   
474  $0$ ,  $\mu_a = 0.96$ . *See separate file for the figure.*

475

### 476 **2.5: Explanation of spectral changes with stochasticity**

477 This section gives the details of: 1) the approximation made to apply linearization theory  
478 to the treatment with  $c_{pa} = 0$ ; and 2) the experimental support for the proposed  
479 mechanisms behind the spectral changes depicted in Fig. 4.

480

481 Application of linearization theory to the  $c_{pa}=0$  treatment:

482 The main text notes that linearization theory cannot immediately explain peak-  
483 change patterns for  $c_{pa}=0$  because the square-root-scale LPA model with  $c_{pa}=0$  has a non-  
484 finite attractor. However, the components of the attractor,  $\sqrt{c_1}$  and  $\sqrt{c_2}$ , can substitute  
485 for a stable 2-point attractor. If  $\mathbf{x}_t$  and  $\mathbf{x}_{t+1}=f(\mathbf{x}_t)$  are square-root-scale population vectors  
486 in  $\sqrt{c_1}$  and  $\sqrt{c_2}$ , respectively, then the product of Jacobians  $S_{\mathbf{x}_t} = J_{\mathbf{x}_{t+1}} J_{\mathbf{x}_t}$  approximates  
487 a susceptibility matrix because  $\mathbf{x}_{t+2}$  is close to  $\mathbf{x}_t$ . Using 5000 points  $\mathbf{x}_t$  covering  $\sqrt{c_1}$ , the  
488 coefficient of variation of each matrix entry of  $S_{\mathbf{x}_t}$  was never more than 7.9%. The  
489 matrices  $S_{\mathbf{x}_t}$  all had similar eigenvalue and eigenvector structure. A negative eigenvalue  
490  $-0.12 \leq d_1 \leq -0.15$  always occurred (mean value -0.13); a complex-conjugate pair of  
491 eigenvalues  $\text{rexp}(\pm i\theta)$  with  $0.97 \leq r \leq 1.03$  and  $40.8^\circ \leq \theta \leq 47.7^\circ$  always occurred (mean  
492  $\theta$  was  $44.4^\circ$ , mean  $r$  was 0.999). The dominant eigenvalue was always complex, with  
493 mean phase angle  $44.4^\circ$ , so theory predicts a component of oscillatory decay of  
494 perturbations from the stable attractor of the square-root-scale model, and corresponding  
495 spectral peaks in the adult life stage at n.f.  $44.4^\circ/(180^\circ \cdot 2) = 0.123$  and  
496  $(360^\circ - 44.4^\circ)/(180^\circ \cdot 2) = 0.877$ . The magnitude of the negative eigenvalue is small, and its  
497 corresponding eigenvector is almost perpendicular to the largest component of stochastic  
498 perturbations that affected the *Tribolium* system, so theory predicts that the  
499 corresponding stochastically-induced spectral peak will not be noticeable. Predicted  
500 stochastically-induced peaks are in the same place as deterministic model peaks. Linear  
501 theory predicts that locations of spectral peaks for  $c_{pa}=0$  will not change with the addition  
502 of stochasticity.

503 For  $c_{pa}=0$ , linearization theory predicted changes in spectral peaks correctly for  
504 weak noise but incorrectly for stronger noise: the main (deterministic) LPA model peaks  
505 at 0.123, 0.887 and 1 were not greatly affected by weak demographic stochasticity (log  $\Sigma$   
506 factors less than about -2.5), but were shifted unexpectedly for larger  $\Sigma$  factors (Fig. 4B).  
507 How can peak motion for higher  $\Sigma$  factors be explained? We answer this question in Fig.  
508 11 below, and in the main text.

509

510 Experimental support for spectral changes:

511 We supported the theoretically-proposed mechanism producing the n.f. 0.33  
512 spectral peak for  $c_{pa} = 0.5$  with experimental data by examining perturbations of real  
513 population vectors from points in the LPA model attractor (Fig. 11A).

514 The LPA model with  $c_{pa}=0$  had an unstable equilibrium,  $e$ , about midway  
515 between  $c_1$  and  $c_2$ . The distance from any population vector to the attractor comprised of  
516  $c_1$  and  $c_2$  was defined to be the minimum distance to any point in the attractor. For a  
517 range of  $\Sigma$  factors, means and 2.5<sup>th</sup> and 97.5<sup>th</sup> percentiles of this minimum distance were  
518 computed across all population vectors in a model-generated time series (Fig. 11B).  
519 Spectral peaks began to move for about the same  $\Sigma$  factors that 97.5<sup>th</sup> percentiles of  
520 distance distributions exceeded the distance between  $e$  and the attractor (Fig. 4B). Peaks  
521 began to shift when stochasticity was strong enough to move population vectors  
522 occasionally at least as far from  $c_1$  and  $c_2$  as  $e$ . Linearization theory failed when this  
523 occurred because linearization at points in the attractor does not capture the dynamical  
524 behavior of the LPA model at points farther from the attractor than  $e$ .

525 For weak stochasticity, the SD-LPA model initialized with a population vector  
526 near  $c_i$  will produce in one time step a vector nearer  $c_j$  ( $j \neq i$ ) than  $c_i$ . Stronger stochasticity  
527 will cause the model to occasionally produce a vector closer to  $c_i$ , shifting the phase of  
528 the n.f. 1 oscillation of the system (Henson *et al.* 1998). The relative frequency of phase  
529 shifting, as a function of the  $\Sigma$  factor, becomes appreciably greater than 0 for the same  
530 range of  $\Sigma$  factors at which stochasticity becomes strong enough to move populations  
531 further from the attractor than  $e$ , and peak motion begins (Fig. 11C).  
532

533 **Figure 11:** Explanation of peak motion patterns with increasing stochasticity for (A)  $c_{pa}$   
534 = 0.5 and (B, C)  $c_{pa} = 0$  in the SD-LPA model. First panel of (A): for every square-root-  
535 scale experimental population vector  $\mathbf{x}_t$  with both  $\mathbf{x}_t$  and  $\mathbf{x}_{t+3}$  within 10 units of  $\mathbf{a}_1$  (text),  
536 the components  $\mathbf{h}_t$  and  $\mathbf{h}_{t+3}$  of  $\mathbf{x}_t - \mathbf{a}_1$  and  $\mathbf{x}_{t+3} - \mathbf{a}_1$  in the direction of  $\mathbf{v}_1$  were computed,  
537 and the signed length (s.l.) of  $\mathbf{h}_{t+3}$  was plotted against the signed length of  $\mathbf{h}_t$ . Other  
538 panels of (A): same as the first panel but using  $\mathbf{a}_2$ ,  $\mathbf{v}_2$  and  $\mathbf{a}_3$ ,  $\mathbf{v}_3$  respectively. Plotted  
539 linear regression slopes were significantly negative (99% level), and took values greater  
540 than -1, demonstrating over-compensatory decay of perturbations from  $\mathbf{a}_i$  in the direction  
541 of  $\mathbf{v}_i$  in three time steps and supporting the mechanism by which theory explains the peak  
542 at n.f. 0.33 for  $c_{pa} = 0.5$ . (B) The increasing trend gives the mean, across length-1024 SD-  
543 LPA-model-generated time series, of the distance between each population vector and the  
544 attractor comprised of  $c_1$  and  $c_2$ . Vertical bars stretch between the 2.5<sup>th</sup> and 97.5<sup>th</sup>  
545 percentiles; they extend beyond the axes for large  $\Sigma$  factors. The solid horizontal line  
546 gives the distance between  $e$  and the attractor. Means of distances between experimental  
547 population triples and the attractor were 47.7, 51.2, and 48.1 for the three replicates with  
548  $c_{pa} = 0$ , agreeing with simulated values. (C) We used the SD-LPA model with each of a  
549 range of  $\Sigma$  factors to generate 50 time series of length 1024. For each time series, the  
550 percentage of steps at which populations failed to switch from being closer to  $c_1$  to being  
551 closer to  $c_2$  or *vice versa* was calculated. The increasing trend gives mean percentages  
552 across the 50 time series; vertical bars span the 2.5<sup>th</sup> and 97.5<sup>th</sup> percentiles. *See separate*  
553 *file for the figure.*  
554

#### 555 **Supplementary References:**

- 556
- 557 1. Brillinger, D. (2001) *Time Series: Data Analysis and Theory*. Society for Industrial  
558 and Applied Mathematics, Philadelphia.
  - 559 2. Cushing, J.M., Costantino, R.E., Dennis, B., Desharnais, R.A. & Henson, S.M. (2003)  
560 *Chaos in Ecology: Experimental Non-linear Dynamics*. Academic Press, New York.
  - 561 3. Dennis, B., Desharnais, R.A., Cushing, J.M., Henson, S.M., Costantino, R.F. (2001)  
562 Estimating chaos and complex dynamics in an insect population. *Ecological*  
563 *Monographs* **71**(2), 277-303.
  - 564 4. Greenman, J. V. & Benton, T. G. (2005) The frequency spectrum of structured  
565 discrete-time population models: Its properties and their ecological implications.  
566 *Oikos*, 110, 369-389.
  - 567 5. Henson, S. M., Cushing, J. M., Costantino, R. F., Dennis, B., & Desharnais, R. A.  
568 (1998) *Proceedings of the Royal Society of London B*, 265, 2229-2234.
  - 569 6. King, A.A., Costantino, R.F., Cushing, J.M., Henson, S.M., Desharnais, R.A.,  
570 Dennis, B. (2004) Anatomy of chaotic attractor: subtle model-predicted patterns

- 571 revealed in population data. *Proceedings of the National Academy of Sciences of the*  
572 *U.S.A.* **101**, 408-413.
- 573 7. Wiesenfeld, K. (1985) Noisy precursors of nonlinear instabilities. *Journal of*  
574 *Statistical Physics*, 38, 1071-1097.

**Figure 5:** Models of *T. castaneum* population dynamics. The deterministic Larvae-Pupae-Adult model (LPA) is presented in the upper left corner, box [1]. The stochastic demographic Larvae-Pupae-Adult model (SD-LPA) is displayed in the upper right corner, box [2]. The lattice stochastic demographic Larvae-Pupae-Adult model (LSD-LPA) is shown in the lower right corner, box [3]. We consider the LSD-LPA model to be assembled starting with the LPA model, adding stochasticity first, then constraining to integer populations, rather than *vice versa*.  $[x] = \max(x, 0)$ . The trivariate random variables  $E_t = (E_{1t}, E_{2t}, E_{3t})$  were standard normal with covariance matrix  $\Sigma$ , and were independent for different values of  $t$ .

## Deterministic

## Stochastic

Fractional population sizes allowed

LPA

1

$$L_{t+1} = bA_t \exp\left(-\frac{c_{el}}{V} L_t - \frac{c_{ea}}{V} A_t\right)$$

$$P_{t+1} = (1 - \mu_l) L_t$$

$$A_{t+1} = P_t \exp\left(-\frac{c_{pa}}{V} A_t\right) + (1 - \mu_a) A_t$$

2

SD-LPA

$$L_{t+1} = \left[ \sqrt{bA_t \exp\left(-\frac{c_{el}}{V} L_t - \frac{c_{ea}}{V} A_t\right) + E_{1t}} \right]^2$$

$$P_{t+1} = \left[ \sqrt{(1 - \mu_l) L_t + E_{2t}} \right]^2$$

$$A_{t+1} = \left[ \sqrt{P_t \exp\left(-\frac{c_{pa}}{V} A_t\right) + (1 - \mu_a) A_t + E_{3t}} \right]^2$$

Integer population sizes only

A deterministic integer-population model was not used because its asymptotic behavior was unrealistically sensitive to small changes in initial conditions.

3

LSD-LPA

$$L_{t+1} = \text{round} \left( \left[ \sqrt{bA_t \exp\left(-\frac{c_{el}}{V} L_t - \frac{c_{ea}}{V} A_t\right) + E_{1t}} \right]^2 \right)$$

$$P_{t+1} = \text{round} \left( \left[ \sqrt{(1 - \mu_l) L_t + E_{2t}} \right]^2 \right)$$

for the treatments:

$$A_{t+1} = \text{round} \left( P_t \exp\left(-\frac{c_{pa}}{V} A_t\right) \right) + \text{round} \left( (1 - \mu_a) A_t \right)$$

for the control:

$$A_{t+1} = \text{round} \left( \left[ \sqrt{P_t \exp\left(-\frac{c_{pa}}{V} A_t\right) + (1 - \mu_a) A_t + E_{3t}} \right]^2 \right)$$

**Figure 6:** Frequency domain fit between the constrained LSD-LPA model (with no further constraint) and observed adult population time series of (A) length 41 and (B) length 213 from the three experimental replicates with  $c_{pa} = 0.35$ . The heavy dashed lines are data log spectra. Light solid lines give the minimum, the 5<sup>th</sup>, 25<sup>th</sup>, 50<sup>th</sup>, 75<sup>th</sup>, and 95<sup>th</sup> percentiles, and the maximum values at each frequency value of 1000 log spectra of model-generated time series of (A) length 41 and (B) length 213. Triangles highlight the 5th and 95th percentiles. Parameters were optimized for length-41 data in the time domain (Table 2). Fit was similar when parameters optimized for the frequency domain were used (Table 3). Fit with other life stages was similar. Aliasing of fundamental (i.e., non-harmonic) frequencies of population fluctuation is unlikely to have occurred because the biology of *Tribolium* suggests that little fluctuation occurs for  $nf$  greater than 1.

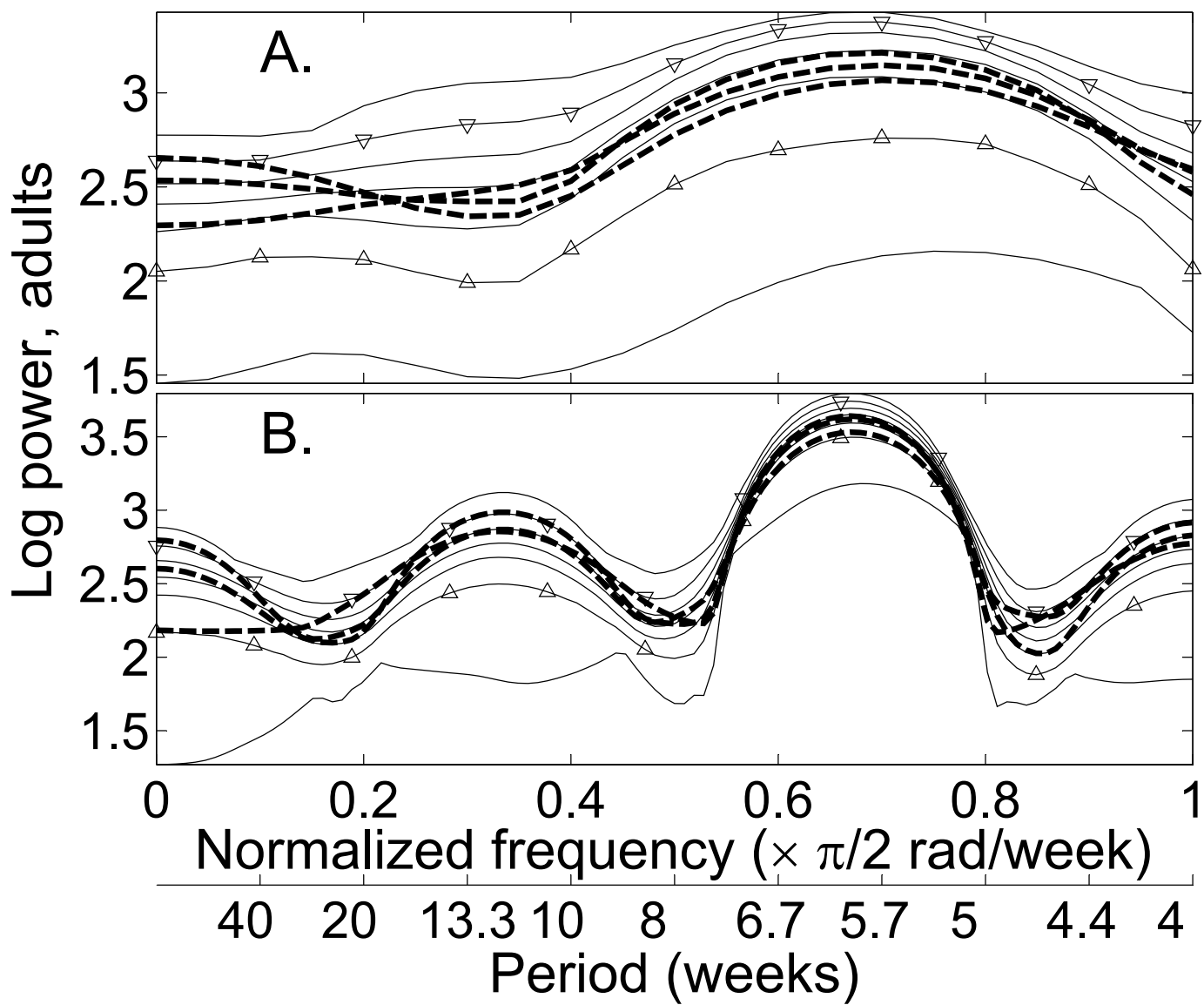
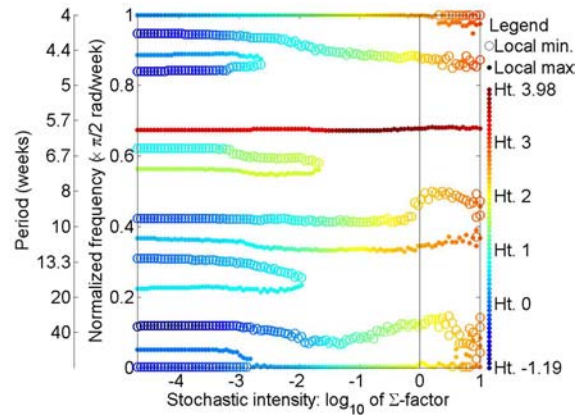
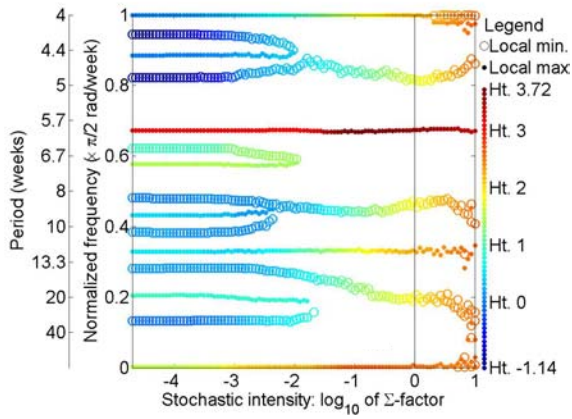
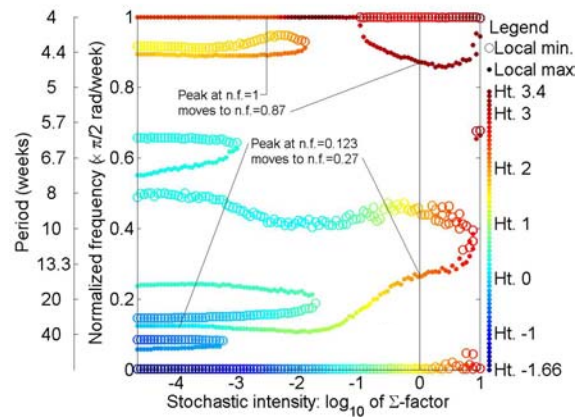
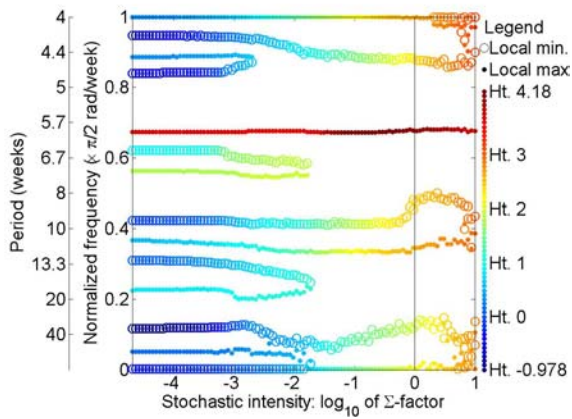


**Figure 7:** (A) Fig. 4A, reproduced here for easy comparison with the other panels. The analog of Fig. 4A for the pupal (B) and larval (C) life stages. (D) Fig. 4B, reproduced for comparison. The analogue of Fig. 4B for the pupal (E) and larval (F) life stages.

**A, B:**



**C, D:**



**E, F:**

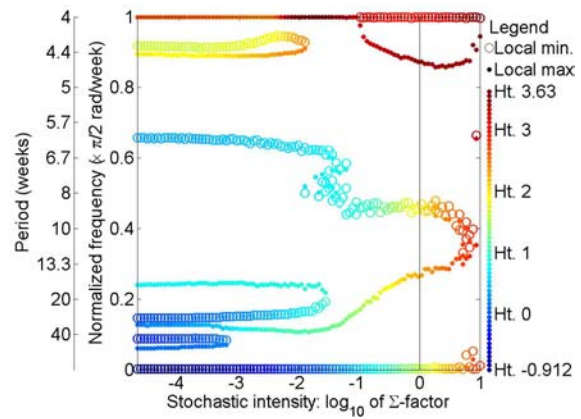
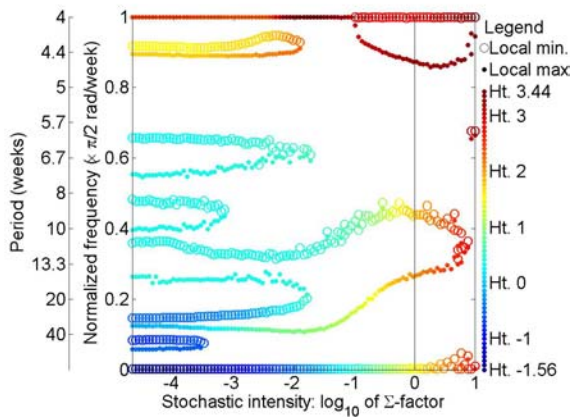
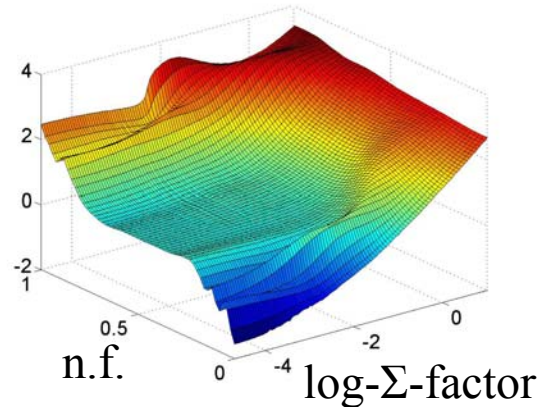
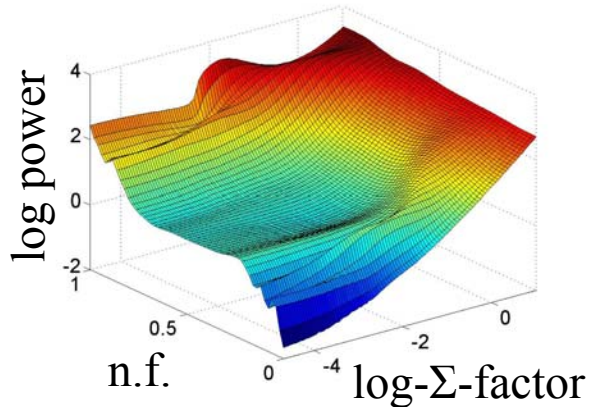


**Figure 8:** Log power versus  $nf$  and  $\log \Sigma$  factor,  $c_{pa} = 0$ ,  $\mu_a = 0.96$ , for the adult (A), pupal (B), and larval (C) life stages. The smoothed median log periodogram estimate was used. As in Fig. 4B and Fig. 7,  $nf = 0$  values have not been plotted. This is the 3-dimensional version of Fig. 4B. There appear to be differences among Figs. 7D-F. This figure shows that the differences are minor; they may not have biological significance.

**A, B:**



**C:**

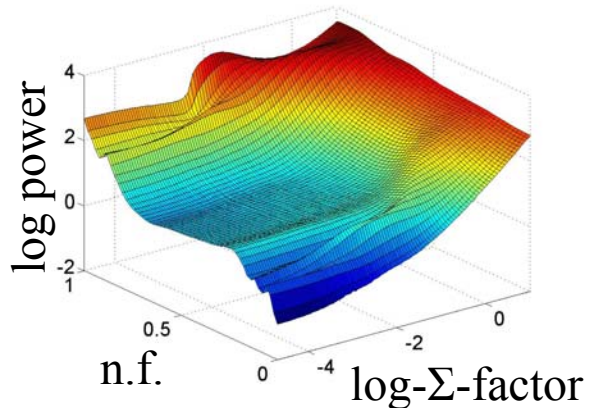
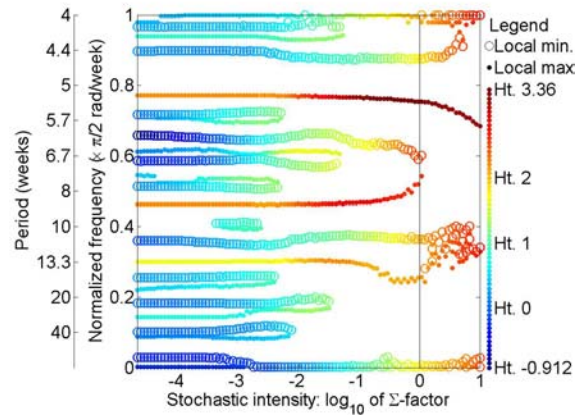
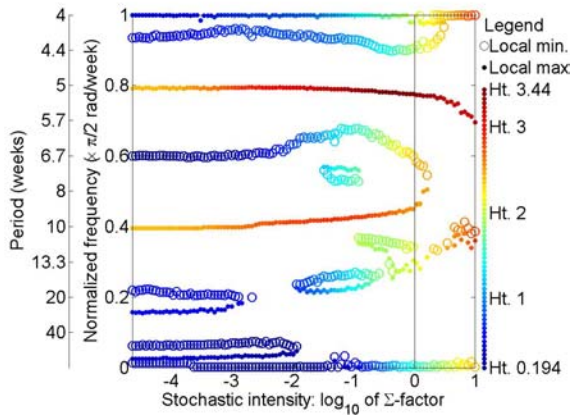
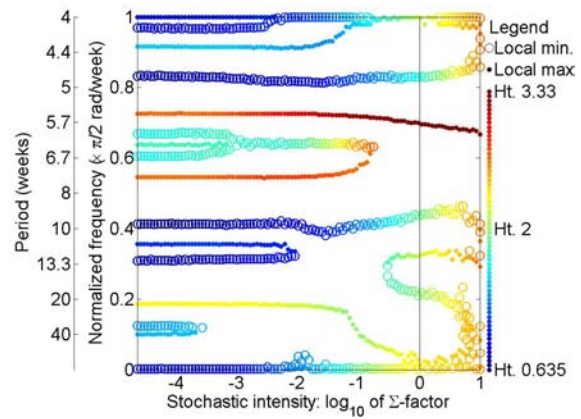
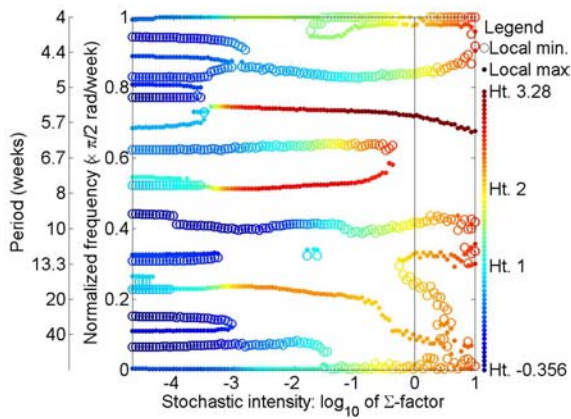


**Figure 9:** Analogues of Fig. 4 for other  $c_{pa}$  values. Adult life stage only.

**A:**  $c_{pa} = 0.05$ ; **B:**  $c_{pa} = 0.1$



**C:**  $c_{pa} = 0.25$ ; **D:**  $c_{pa} = 0.35$



**E:**  $c_{pa} = 1$

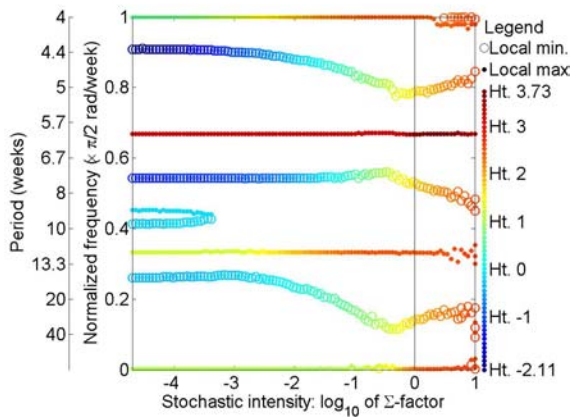


**Figure 10:** The attractor (circles) and unstable equilibrium (x) of the LPA model for  $c_{pa} = 0, \mu_a = 0.96$ .

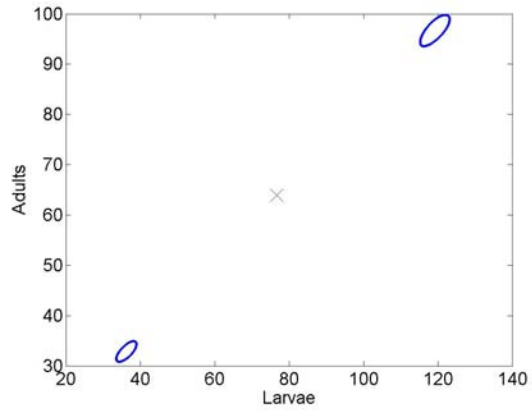


**Figure 11:** Explanation of peak motion patterns with increasing stochasticity for (A)  $c_{pa} = 0.5$  and (B, C)  $c_{pa} = 0$  in the SD-LPA model. First panel of (A): for every square-root-scale experimental population vector  $\mathbf{x}_t$  with both  $\mathbf{x}_t$  and  $\mathbf{x}_{t+3}$  within 10 units of  $\mathbf{a}_1$  (text), the components  $\mathbf{h}_t$  and  $\mathbf{h}_{t+3}$  of  $\mathbf{x}_t - \mathbf{a}_1$  and  $\mathbf{x}_{t+3} - \mathbf{a}_1$  in the direction of  $\mathbf{v}_1$  were computed, and the signed length (s.l.) of  $\mathbf{h}_{t+3}$  was plotted against the signed length of  $\mathbf{h}_t$ . Other panels of (A): same as the first panel but using  $\mathbf{a}_2, \mathbf{v}_2$  and  $\mathbf{a}_3, \mathbf{v}_3$  respectively. Plotted linear regression slopes were significantly negative (99% level), and took values greater than -1, demonstrating over-compensatory decay of perturbations from  $\mathbf{a}_i$  in the direction of  $\mathbf{v}_i$  in three time steps and supporting the mechanism by which theory explains the peak at  $\text{nf } 0.33$  for  $c_{pa} = 0.5$ . (B) The increasing trend gives the mean, across length-1024 SD-LPA-model-generated time series, of the distance between each population vector and the attractor comprised of  $c_1$  and  $c_2$ . Vertical bars stretch between the 2.5<sup>th</sup> and 97.5<sup>th</sup> percentiles; they extend beyond the axes for large  $\Sigma$  factors. The solid horizontal line gives the distance between  $e$  and the attractor. Means of distances between experimental population triples and the attractor were 47.7, 51.2, and 48.1 for the three replicates with  $c_{pa} = 0$ , agreeing with simulated values. (C) We used the SD-LPA model with each of a range of  $\Sigma$  factors to generate 50 time series of length 1024. For each time series, the percentage of steps at which populations failed to switch from being closer to  $c_1$  to being closer to  $c_2$  or *vice versa* was calculated. The increasing trend gives mean percentages across the 50 time series; vertical bars span the 2.5<sup>th</sup> and 97.5<sup>th</sup> percentiles.

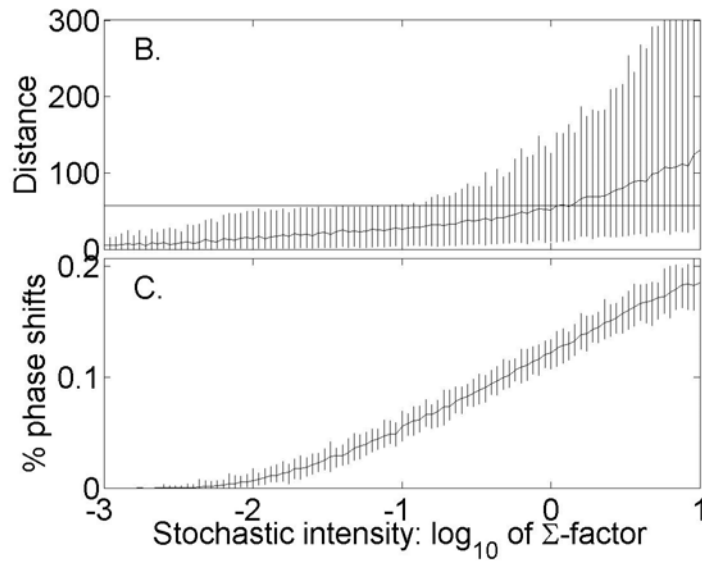
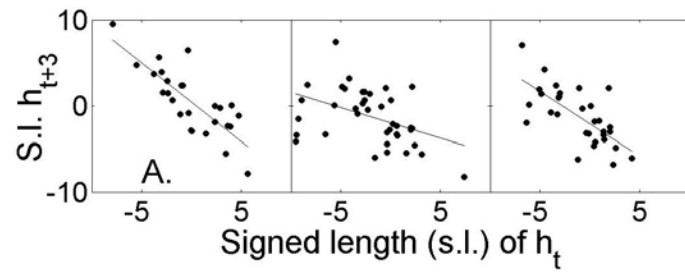


**Table 1:** The parameters used for the models of Fig. 5. These were obtained using time domain fitting methods (Dennis *et al.* 2001, Cushing *et al.* 2003).

Dennis, B., Desharnais, R.A., Cushing, J.M., Henson, S.M., Costantino, R.F. (2001) Estimating chaos and complex dynamics in an insect population. *Ecological Monographs* **71**(2), 277-303.

Cushing, J.M., Costantino, R.E., Dennis, B., Desharnais, R.A. & Henson, S.M. (2003) *Chaos in Ecology: Experimental Non-linear Dynamics*. Academic Press, New York.

Parameter	value	95% confidence intervals
$b$	10.45	(10.04, 10.77)
$\mu_l$	0.2000	(0.1931, 0.2068)
$c_{ea}$	0.01310	(0.01285, 0.01340)
$c_{el}$	0.01731	(0.01611, 0.01759)
$\mu_a$ for the control treatment (replicates 4, 11, and 24)	0.007629	(0.006769, 0.008489)
$\mu_a$ for the non-control treatments	0.96	NA
$c_{pa}$ for the control treatments (reps. 4, 11 and 24)	0.004619	(0.004446, 0.004792)
$c_{pa}$ for reps. 5, 12 and 15	0	NA
$c_{pa}$ for reps. 1, 7 and 20	0.05	NA
$c_{pa}$ for reps. 6, 10 and 16	0.1	NA
$c_{pa}$ for reps. 8, 17 and 21	0.25	NA
$c_{pa}$ for reps. 2, 13 and 22	0.35	NA
$c_{pa}$ for reps. 9, 14 and 19	0.5	NA
$c_{pa}$ for reps. 3, 18 and 23	1	NA
$V$	1 unit, of mass 20 g	NA
$\Sigma$ for the control treatments	$\begin{pmatrix} 1.621 & -0.1336 & -0.01339 \\ -0.1336 & 0.7375 & -0.0009612 \\ -0.01339 & -0.0009612 & 0.01212 \end{pmatrix}$	
$\Sigma$ for the non-control treatments	$\begin{pmatrix} 2.332 & 0.007097 & 0 \\ 0.007097 & 0.2374 & 0 \\ 0 & 0 & 0 \end{pmatrix}$	

**Table 2:** Optimized parameter values. Optimized parameter values in the time domain (column 2), and in the frequency domain according to the spectrum distance fit test (columns 4-8), with respect to the length-41 experimental replicates with  $c_{pa} = 0.35$  only. Values in brackets do not fall within the confidence intervals in column 3. Time-domain fitting used the maximum likelihood one-step forecasting methods of Dennis *et al.* (2001). Frequency-domain optimization used an adaptation of the Nelder-Mead simplex algorithm to minimize the distance between the mean log spectrum of model-generated time series and data log spectra. The time-domain-optimal parameters (column 2) were used as initial conditions. Confidence intervals for the time-domain-optimal parameters other than  $\Sigma$  were computed as in Dennis *et al.* (2001). Confidence intervals for entries of  $\Sigma$  were computed by re-sampling (with replacement) from the set of residuals of data from one-step forecasts of the model with time-domain-optimal parameters.

Dennis, B., Desharnais, R.A., Cushing, J.M., Henson, S.M., Costantino, R.F. (2001) Estimating chaos and complex dynamics in an insect population. *Ecological Monographs* **71**(2), 277-303.

	Time domain optim.	99% confidence intervals	Frequency domain optimization				
			Run 1	Run 2	Run 3	Run 4	Run 5
Constrained LSD-LPA model							
$b$	10.34	(8.691, 12.00)	10.5145	9.8131	10.393	9.5343	10.4432
$c_{el}$	0.0158	(0.01258, 0.01919)	[0.0112]	0.0187	[0.0105]	[0.0104]	[0.0118]
$c_{ea}$	0.0131	(0.01177, 0.01429)	0.0137	0.0127	0.0133	0.0127	0.0137
$\mu_l$	0.163	(0.1336, 0.1850)	0.1641	[0.1867]	[0.1863]	0.164	0.1519
$\Sigma(1,1)$	1.852	(1.134, 2.725)	2.3439	[3.6852]	[2.7508]	[3.0581]	2.2219
$\Sigma(2,2)$	0.2391	(0.09616, 0.5066)	0.2304	[0.06]	0.2014	0.2097	0.2441
Constrained LSD-LPA with $c_{ea}=0$							
$b$	1.515	(0.7590, 1.785)	1.554	1.5319	1.5578	1.5513	1.5611
$c_{el}$	0.0057	(0.0005164, 0.01140)	0.0059	0.0061	0.006	0.0058	0.0062
$\mu_l$	0.163	(0.1280, 0.1915)	0.1571	0.1535	0.1597	0.1558	0.1582
$\Sigma(1,1)$	13.25	(8.334, 19.43)	13.5359	13.7074	13.3708	13.5479	14.3979
$\Sigma(2,2)$	0.2391	(0.1005, 0.4948)	0.2364	0.2347	0.2375	0.2422	0.2147
Constrained LSD-LPA with $c_{el}=0$							
$b$	4.199	(3.084, 5.949)	[6.2564]	5.5148	[6.1404]	[6.3951]	[6.179]
$c_{ea}$	0.0085	(0.006145, 0.01212)	0.0094	0.008	0.0093	0.0096	0.0094
$\mu_l$	0.163	(0.1331, 0.1856)	0.1432	[0.2039]	0.1435	0.1387	0.1405
$\Sigma(1,1)$	8.885	(5.432, 13.63)	3.4277	3.2261	3.4572	3.2865	2.9952
$\Sigma(2,2)$	0.2391	(0.09452, 0.5036)	0.2152	0.2788	0.2143	0.2349	0.2177

**Table 3:** Frequency domain fit of models with  $c_{pa} = 0.35$  data. Parameters are specified in Table 2. Table entries are P values as given by the spectrum distance fit test (columns 2-3) and the spectrum shape fit test (columns 4-5). They describe the fit between models and length-41 (columns 2, 4) or length-213 (columns 3, 5) versions of the three  $c_{pa} = 0.35$  experimental time series.

Parameters	Spectrum dist. P val., length 41	Spectrum dist. P val., length 213	Spectrum shape P val., length 41	Spectral shape P val., length 213
Constrained LSD-LPA model				
Time domain	0.6303 0.8007 0.9408	0.2994 0.0750 0.3072	0.1822 0.6871 0.6374	0.1903 0.0484 0.1297
Freq. dom., run 1	0.7523 0.8404 0.9322	0.1338 0.0867 0.1421	0.2168 0.6143 0.8441	0.2695 0.1900 0.3256
Freq. dom., run 2	0.8329 0.9365 0.8744	0.0934 0.1057 0.1431	0.2842 0.6658 0.8075	0.0261 0.0238 0.0551
Freq. dom., run 3	0.7740 0.8781 0.9209	0.1868 0.1799 0.2362	0.2632 0.5810 0.9026	0.0696 0.0617 0.0988
Freq. dom., run 4	0.7984 0.8827 0.9390	0.0998 0.1558 0.1817	0.3036 0.5402 0.9291	0.0304 0.0419 0.0576
Freq. dom., run 5	0.7213 0.8226 0.9488	0.3033 0.1846 0.3531	0.2124 0.6241 0.8250	0.1540 0.0812 0.1529
Constrained LSD-LPA with $c_{ea} = 0$				
Time domain	0.7425 0.7277 0.6565	0.0543 0.0692 0.0571	0.2996 0.2601 0.2752	0.0001 0.0001 0.0001
Freq. dom., run 1	0.7991 0.7933 0.7233	0.0423 0.0535 0.0434	0.2826 0.2434 0.2622	0 0 0
Freq. dom., run 2	0.7795 0.7707 0.6942	0.0448 0.0560 0.0458	0.2855 0.2485 0.2669	0 0 0
Freq. dom., run 3	0.7918 0.7828 0.7145	0.0393 0.0498 0.0401	0.2772 0.2402 0.2593	0 0 0
Freq. dom., run 4	0.7863 0.7797 0.7076	0.0432 0.0531 0.0434	0.2790 0.2450 0.2610	0 0 0
Freq. dom., run 5	0.8024 0.7982 0.7233	0.0356 0.0459 0.0364	0.2752 0.2359 0.2569	0 0 0
Constrained LSD-LPA with $c_{el} = 0$				
Time domain	0.1766 0.1715 0.0895	0 0.0005 0.0001	0.2562 0.2543 0.2467	0 0 0

Freq. dom., run 1	0.2060 0.2345 0.1202	0.0009 0.0045 0.0017	0.2389 0.1778 0.2571	0 0.0003 0.0002
Freq. dom., run 2	0.2130 0.2509 0.1223	0.0001 0.0002 0.0002	0.1816 0.1496 0.1751	0 0 0
Freq. dom., run 3	0.2105 0.2386 0.1170	0.0003 0.0029 0.0008	0.2263 0.1712 0.2410	0 0.0001 0
Freq. dom., run 4	0.2039 0.2263 0.1224	0.0006 0.0056 0.0019	0.2560 0.1884 0.2795	0.0001 0.0004 0.0001
Freq. dom., run 5	0.2018 0.2252 0.1174	0.0004 0.0033 0.0017	0.2234 0.1702 0.2317	0 0 0